Ni-NbOx Bifunctional Catalysts for Selective Hydrodeoxygenation of m-Cresol to Toluene

Camila Abreu Teles, Carmen Ciotonea, Ruben Palacio, Diana Lopez, Sébastien Royer, Frédéric Richard

Ni–NbO_x Bifunctional Catalysts for Selective Hydrodeoxygenation of m-Cresol to Toluene

Camila A. Teles[1,*], Carmen Ciotonea[2], Ruben Palacio,[3] Diana Lopez,[3] Sébastien Royer[2], Frédéric Richard[1]

[1] *Université de Poitiers, CNRS, Institut de Chimie des Milieux et Matériaux de Poitiers, UMR 7285, rue Michel Brunet, BP633, 86022 Poitiers, France.*

[2] *Université du Littoral Côte d'Opale, Unité de Chimie Environnementale et Interactions sur le Vivant-UCEIV, UR4492, 59140 Dunkerque, France.*

[3] *Química de Recursos Energéticos y Medio Ambiente, Instituto de Química, Facultad deCiencias Exactas y Naturales, Universidad de Antioquia UdeA; Calle 70 No. 52-21, Medellín, Colombia.*

* Corresponding author: camila.abreu.teles@univ-poitiers.fr

Submitted to Molecular Catalysis

August 2025

Abstract

The catalytic performances of a series of Ni supported on mesoporous silica (SBA-15) and niobia, as well as Ni-NbO_x dispersed on SBA-15 were evaluated for the hydrodeoxygenation (HDO) of m-cresol at 300 °C under atmospheric pressure. Under the reaction conditions, hydrogenation and C-C hydrogenolysis pathways yielding only oxygenated products dominated over the monometallic Ni catalyst. In contrast, the Direct DeOxygenation pathway (DDO) leading to toluene was significantly promoted when Ni was in contact with oxophilic NbO_x surface. Tuning the Ni-Nb ratio on silica revealed a remarkable enhancement of the DDO rate constant. Indeed, the kinetic rate constant determined over 5Ni5Nb/SBA was about 11 times higher than that measured on the catalyst containing only the Ni phase. This enhanced performance can be attributed to the formation of well-dispersed Ni–NbO_x interfacial sites, where the hydrogenation capability of Ni associate with the oxophilic character of Nb^{5+}/Nb^{4+} species allowing to a more efficient activation of the C-O bonding and promoting the DDO reaction pathway. These results offer valuable insights for the rational design of selective catalysts for the transformation of lignin-derived bio-oils into aromatic hydrocarbons.

Keywords: Biomass, hydrodeoxygenation; SBA-15; Ni/NbO_x site interface

1. Introduction

Lignocellulosic biomass is nowadays one of the most important sources of renewable feedstock to the production of biofuels and bio-based products. Particularly, lignin fraction is a rich source of aromatics compounds that can be converted into a promising liquid fuel (bio-oil) for use in transport engines, through the fast pyrolysis process. However, this liquid cannot be directly used due to its poor quality related to the high content of oxygen [1,2]. Catalytic conversion of those oxygenated products, mostly phenolic compounds, can be achieved by the hydrodeoxygenation (HDO) process. Herein, the challenge is to develop suitable catalysts, able to promote the selective formation of deoxygenated products with a minimum consumption of hydrogen, hence aromatic compounds like BTX (Benzene, Toluene, Xylene) products.

Co-Mo and Ni-Mo sulphated catalyst, traditionally used for the hydrotreatment process, can efficiently reduce the oxygen content in the bio-oil [3,4]. However, due to their instability under reaction and the requirement of sulfur in the stream to preserve the active phase, alternative catalyst formulations have been proposed. Among these, bifunctional catalysts combining of metallic phase with oxophilic sites appears to efficiently promote deoxygenation of model phenolic compounds such as phenol, cresols and anisole [5–11]. The efficiency of such catalytic systems arises from to the activation of the oxygen atom at the oxophilic sites located near the metal particles, followed by selective hydrogenation/hydrogenolysis activated by the metal, thus producing aromatic products. This has been reported to happen over a series of noble metals such as Pt, Pd, Rh, Ru on oxophilic support such as ZrO_2, TiO_2, Nb_2O_5 [9,12–19]. Among them, niobia-supported catalysts stand out with higher activity and selectivity toward deoxygenated products. Teles et al. have investigated a series of Pd supported on various oxides (SiO_2, CeO_2, ZrO_2, TiO_2 and Nb_2O_5)

on the HDO reaction of phenol, m-cresol and anisole at 300 °C under atmospheric pressure [13]. The product distribution significantly varied with the support type. While Pd supported on SiO_2 and CeO_2 favored the formation of the hydrogenated product (methyl)-cyclohexanone, supports like ZrO_2, TiO_2 and Nb_2O_5 promoted the formation of benzene/toluene, with selectivity following the order Pd/Nb_2O_5 > Pd/TiO_2 > Pd/ZrO_2 >> Pd/CeO_2 ~ Pd/SiO_2, regardless the model compound. The higher deoxygenation activity of Pd/Nb_2O_5 catalyst was explained by its superior oxophilicity, which strongly interact with the oxygen atom of the oxygenated organics, thus facilitating the C-O bond cleavage or selective hydrogenation of C=O bond. Rezende et al., in turn, investigated different metals (Pt, Rh and Ni) supported on the same Nb_2O_5 support in the HDO of phenol at 300°C and P_{H2} = 1bar [20]. All of catalysts exhibited comparable selectivity to benzene (ranging from 92 to 97 %). However, when the NiO phase was fully reduced (activation at 500 °C), the HDO rate decreased, likely due to the strong metal-support (SMSI) effect, which led to partial coverage of the Ni metal particles. Surprisingly, a different behavior was observed when a $Pt/Nb_2O_5/MgAl_2O_4$ catalyst was evaluated in HDO of m-cresol at 350 °C under atmospheric pressure [21]. Indeed, after the catalyst reduction at 500 °C, Pt was encapsulated by the partially reduced NbO_x species, leading to the improvement of activity (by 47.5 % instead of 10%) and selectivity to toluene (98% instead of 87%) compared to Pt on non-SMSI support ($Pt/MgAl_2O_4$). The promoting effect of NbO_x species on the Pt based catalysts was also demonstrated by Chen et al. [22]. In that study, the activity of Pt/C and NbO_x-modified Pt catalysts was evaluated for the HDO of m-cresol at 350 °C under atmospheric pressure. The NbO_x–Pt/C catalyst exhibited an enhanced selectivity to toluene (95%), which was attributed to the interaction of the hydroxyl group of m-cresol with uncoordinated Nb cations. This adsorption mode, with the aromatic ring tilted away from the surface, favored the direct deoxygenation pathway. Moreover, interactions at the NbO_x–Pt interface were proposed to

stabilize NbO_x in its partially reduced state. A similar promoting effect on toluene selectivity has also been reported for WO_x-decorated Pt catalysts, where Pt stabilizes the WO_x film while facilitating the generation of oxygen vacancies [23,24]. In this case, HDO of m-cresol proceeds via direct C–O bond cleavage of molecules adsorbed on the oxygen vacancies of the WO_x species. These studies may imply that the active sites for deoxygenation, *i.e.*, metal-oxophilic interfaces, are created when the NbO_x overlayes on the metal surface. However, in the case where higher catalyst activation temperatures are needed, the extension of NbO_x migration may needs to be controlled to avoid excessive loss of exposed metal surface area, thus decreasing the interface perimeter and consequent loss of HDO activity.

The main objective of the present study was to examine the performance of Ni-NbO_x species interface in the gas phase HDO reaction of m-cresol. As the niobium oxide is a reducible support that promote the SMSI effect, a Ni-Nb_2O_5 system deposited on silica surface was proposed in order to maximize metal-oxophilic sites interface and minimize Ni surface coverage. SBA-15 was chosen as silica support owing to its high surface area and ordered channel-type mesopores, allowing the accommodation of reactant and the control of metal particle size [25,26]. A series of catalysts varying the content of Ni and Nb was prepared, characterized and evaluated in the HDO reaction of m-cresol at 300 °C under atmospheric pressure (fixed bed configuration).

2. Experimental Section

2.1. Support Preparation

For the preparation of the support SBA-15, P123, used as a structure-directing agent, was solubilized in a 1.6 M HCl solution at 40 °C with stirring. The silicon source (TEOS) was then added dropwise, and the solution was continuously stirred at 40 °C during 2 h. The resulting mixture was then submitted to a hydrotreatment in a Teflon-lined autoclave at 100

°C for 48 h. Afterward, the precipitated was recovered by filtration, washed with deionized water, and dried at 100 °C for 24 h. The resulting solid was then calcined at 550 °C for 6 h (heating ramp of 1.5 °C min^{-1}) to remove the organic template. The support was denoted as SBA-15. Nb_2O_5 support was obtained by calcination of niobic acid (CBMM) at 500 °C (1.5 °C min^{-1}) for 6 h.

2.2. Catalyst Preparation

Ni and/or NbO_x supported on SBA-15 and Nb_2O_5 catalysts were prepared by the melt infiltration (MI) of Ni nitrate. In this procedure, the precursor $Ni(NO_3)_2.6H_2O$ was gentle ground with the supports at ambient conditions. The resulting powder was further treated in a teflon autoclave at the melting point of the precursor (57 °C) during 4 days. For the preparation of Ni-NbO_x supported materials, niobium oxalate ($NH_4[NbO(C_2O_4)_2(H_2O)_2].nH_2O$) and nickel nitrate were ground together with the respective supports and submitted to the same thermal treatment at 57 °C. The materials were further calcined in a muffle at 500 °C (1.5 °C min^{-1}) for 6 h to obtain the supported catalysts and afterwards, pelleted, crushed and sieved (200-315 μm). The catalysts were prepared by varying the content of nickel and niobium and were denoted by xNiyNb/SBA where x and y varied between 2.5 and 5 wt.%.

A 5 wt.% of Ni supported on Nb_2O_5 was also prepared by the same MI procedure, followed by calcination at the conditions previously described. This sample was denoted as 5Ni/Nb_2O_5.

2.3. Catalyst Characterization

Both Ni and Nb contents were determined by inductively coupled plasma optical emission spectroscopy (ICP-OES). Analyses were performed on a SPECTRO ARCOS ICP-OES

instrument. Before analysis, the samples were digested using concentrated nitric acid and hydrofluoric acid on a microwave heating system.

The textural properties of the materials were determined by N_2 physisorption at -196 °C using a Micromeritics Tristar II automated gas sorption system. Before analysis, the samples were outgassed under dynamic vacuum at 240 °C for 3 h. Specific surface areas were determined using the multipoint B.E.T. algorithm, in the 0.10 – 0.25 P/P_0 interval. The pore volume and mesopore size distribution were determined using the B.J.H. method from the desorption branch of the isotherms.

Small and wide-angle X-ray diffraction (XRD) analysis of the materials were obtained using a PAN-analytical EMPYREAN powder diffractometer in Bragg-Brentano configuration with Cu Kα radiation (λ = 0.154 nm, 45 kV, 40 mA) in the 10–80° 2θ range with a 0.02° 2θ step. Phase identification was performed by comparison with the ICDD database. The XRD patterns of the supported catalysts were obtained for the samples after *ex situ* activation at 500 °C, 5 °C min^{-1}, under pure hydrogen flow (50 ml min^{-1}) for 1 h.

The reducibility of the materials was studied by H_2-TPR. The analyzes were performed on a Micromeritics AutoChem 2910 from room temperature to 1000 °C, using a heating ramp of 10 °C min^{-1}, under 10 vol.% of H_2 in Ar flow (flow rate of 30 mL min^{-1}). Prior to the TPR run, the samples were pretreated wit pure oxygen (30 mL min^{-1}) at 400 °C during 1 h. The hydrogen consumption was monitored using a TCD detector.

The morphology of bare SBA-15 and dispersion of Ni and Nb species were analyzed by transmission electron microscopy (TEM) using a TITAN Themis 3007 S/TEM. The instrument was equipped with a high brightness Schottkey field emission gun, a probe aberration corrector, super-X detector system with four windowless silicon drift detectors for electron dispersive X-ray spectroscopy (EDX), and several annular dark field detectors. Experiments were conducted at 300 kV with semi-convergence angle of about 20 mrad, a

probe size of the order of 500 pm and a probe current at around 100 pA. For high-angle annular dark field (HAADF) imaging, the camera length was adjusted to yield collection angles between 50 and 200 mrad. The EDX mapping was performed in multi-frame spectrum imaging mode with dwell time per pixel of about 15 µs and continuously scanning until a total acquisition time of 15-20 minutes was achieved. The samples were reduced *ex-situ* under pure H_2 flow (50 mL min^{-1}) at 500 °C (5 °C min^{-1}) during 1 h and then embedded in a polymeric resin, sliced into 50 nm-thick sections using an ultramicrotome and further deposited on a carbon grid for analysis. The software ImageJ version 1.8 was used to analyze the images and to plot particle size histograms.

CO chemisorption analysis was performed in order to determine Ni dispersion. The samples were firstly reduced at 500 °C (5 °C min^{-1}), under pure hydrogen flow (30 mL min^{-1}) for 1 h. The reactor was then cooled down to the adsorption temperature (30 °C) under helium (30 mL min^{-1}). Successive pulses of pure CO (0.465 mL) were injected into the reactor each 3 min. The quantification of chemisorbed CO was carried out using a gas phase chromatograph equipped with a TCD detector and a Porapak Q column. A CO/Ni ratio of 1 was considered.

The acidity of the catalysts was measured by DRIFTS of adsorbed pyridine. Experiments were conducted on a Nicolet Nexus instrument equipped with a DTGS detector and a quartz cell with CaF_2 windows. The samples were first reduced at 500 °C under flow of pure hydrogen for 1 h and then, cooled down to 150 °C, where a spectrum was registered as reference. Pyridine adsorption was carried out during 5 min, with a further vacuum purge during 1 h. Spectra were recorded between 150 and 450 °C at a resolution of 2 cm^{-1} and accumulating 64 scans bet.

Thermogravimetric analysis (ATG) of spent catalysts was performed in order to investigated the deposition of carbonaceous species over the catalysts during the HDO reaction. The measurements were carried out on a SDT Q600 TA Instruments apparatus. The

analysis was performed in the temperature range of 25 °C up to 1000 °C, 10°C min^{-1}, under flow of 100 mL min^{-1} of synthetic air.

2.4. Catalytic transformation of m-cresol

Vapor phase HDO reaction of m-cresol was conducted in a fixed-bed flow reactor system, operating at 300 °C under atmospheric pressure. The carrier gas flow rate was 50 mL min^{-1} of H_2 and a H_2/m-cresol molar ratio was fixed at 80. Before reaction, the catalysts were reduced with pure hydrogen (50 mL min^{-1}) at 500 °C for 1 h. The temperature was then cooled to the reaction temperature (300 °C) and the flow of hydrogen and m-cresol adjusted to different contact times in order to obtain m-cresol conversion around 10 % to ensure differential conditions. The reactant feedstock, introduced at the top of the reactor by using a push-syringe, was composed by m-cresol (7 mol %), decane (3 mol %; used as internal standard), and n-heptane as a solvent. The line at the bottom of the reactor was maintained at 5 °C using a Minichiller-Huber condenser, in order to condense any unconverted reactant and products. The liquid samples were collected at 0.5 h and analyzed by a Varian 430 chromatograph equipped with a DB-5 capillary column and a flame-ionization detector (FID). The conversion of m-cresol and product selectivity for each product were calculated using eqs. (1) and (2):

$$\mathbf{X\ (in\ \%)} = \frac{\mathbf{n^0_{m-cresol} - n_{m-cresol}}}{\mathbf{n^0_{m-cresol}}} \times \mathbf{100} \qquad (1)$$

$$\boldsymbol{S_i}\ \mathbf{(in\ mol\ \%)} = \frac{\mathbf{n_i}}{\mathbf{n^0_{m-cresol} - n_{m-cresol}}} \times \mathbf{100} \qquad (2)$$

Where $n^0_{m\text{-}cresol}$ and $n_{m\text{-}cresol}$ are the number of moles of m-cresol in the beginning and after 0.5 h of reaction, respectively; n_i is the number of moles of a given *i* product.

Assuming a pseudo-first-order reaction, the total kinetic rate constant (k_{TOT} in mmol g_{Ni}^{-1} h^{-1}) and the kinetic rate constants for the different reactions pathways proposed were calculated using the equations (3) and (4):

$$\mathbf{k_{TOT}\ (in\ mmol\ g_{Ni}^{-1}\ h^{-1})} = \frac{-F\ Ln\ (1-X)}{\mathbf{w}.(\%\mathbf{Ni})} \quad (3)$$

$$\mathbf{k_y (in\ mmol\ g^{-1}\ h^{-1})} = r_{TOT}.S_y \quad (4)$$

Where k_{TOT} is the total kinetic rate constant calculated for the global transformation of m-cresol and k_y are the kinetic rate constants for the different reaction pathways; X is the m-cresol conversion; F is the m-cresol molar flow rate (in mmol h^{-1}); w is catalyst weight (in g), %Ni is the Ni content measured by ICP-OES and S_y is the selectivity to the different products: toluene for the deoxygenation route (DDO), 3-methylcyclohexanone, 3-methylcylohexanol, methylcyclohexene isomers and methylcyclohexane for the hydrogenation route (HYD), phenol and benzene for the hydrogenolysis route (HYG).

3. Results and Discussion

3.1. Nickel supported on SBA-15 and Nb_2O_5 catalysts

3.1.1 Characterization results

Small-angle XRD pattern of the SBA-15 and wide-angle XRD patterns of the Ni supported catalysts after reduction (500 °C, 1h) are shown in Figs. 1a and S1. The small-angle XRD pattern showed three main diffraction peaks corresponding to the (100), (110), and (200) reflections, which are characteristic of the highly ordered hexagonal 2D pore structure of SBA-15 with P6mm symmetry, thus confirming the successful synthesis of the material. Besides that, the presence of (210) and (300) reflections is a clear indication of a long-range mesopore ordering and the good textural uniformity of the SBA-15. The SBA-15 supported

catalyst exhibited a broad signal centered at 22.6°, typical of amorphous silica, and two diffraction lines at 44.5 and 51.9° corresponding to (111) and (200) planes of Ni metallic phase (PDF 04-0850). For the niobia supported catalyst, it is observed a set of intense diffraction lines, characteristic of pseudohexagonal TT-Nb_2O_5 (JCPDS: 28-0317). In addition, a weak diffraction peak at 44.5° is observed, corresponding to the metallic Ni(0) phase. Ni particles size was calculated using the Scherrer equation, being obtained approximately the same (around 8 nm) for both 5Ni/SBA and 5Ni/Nb_2O_5 samples.

The textural properties of the calcined samples were evaluated by N_2 physisorption. The adsorption/desorption isotherms (Fig. S2) for the bare SBA-15 supported and after NiO introduction, showed a type IVa isotherm, characteristic of mesoporous materials and a H1-type hysteresis, indicating the presence of cylindrical (tubular) pores as awaited for the SBA-15 material. For the niobia-supported catalyst, a type IV – type II mixed isotherm was observed, indicating the presence of mesopores, however without saturation plateau and resulting in wider pore size distribution. As expected, a high surface area was obtained for SBA-15 support (754 $m^2\ g^{-1}$), while much lower value is obtained for Nb_2O_5 (60 $m^2\ g^{-1}$). The surface area of niobium oxide strongly varies with calcination temperature and the crystallography phase formed. A low surface area is commonly reported in the literature for calcination at temperatures above 500 °C [27,28]. Upon introduction of NiO, both samples showed reasonable decrease in the surface area (< 14 and 32% for Ni/SBA and Ni/Nb_2O_5 respectively), which is associated to the denser NiO phase in the solid.

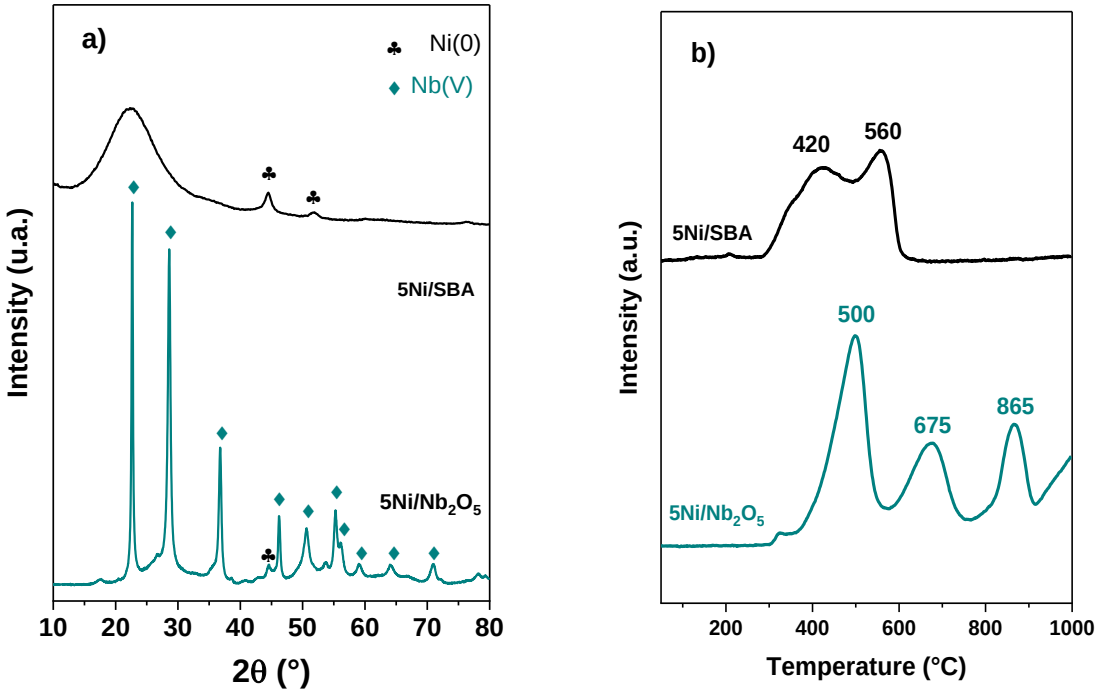

Figure 1. a) XRD patterns of the reduced 5Ni/SBA and 5Ni/Nb_2O_5 samples and b) H_2-TPR profile of the respective calcined samples.

H_2-TPR analysis was performed to assess the reducibility of the samples (Fig. 1b). For 5Ni/SBA, two reduction phenomena are observed at around 420 and 560 °C, corresponding to the reduction of bulky NiO particles located at the external surface of SBA-15, and NiO mesopores confined NPs, respectively. In the latter case, the higher temperature (520 °C) may be likely to the presence of multiple chained particles in the same pore, thus reducing the reduction rate [25]. In the case of 5Ni/Nb_2O_5 sample, a more complex reduction profile is observed. A first reduction peak centered at 500 °C may be associated to the reduction of NiO in strong interaction with Nb_2O_5 support, as previously reported [5,29]. The hydrogen consumption observed at higher temperatures, 675 °C and 865 °C, may be assigned to the reduction surface and bulk Nb_2O_5 to NbO_2, respectively, facilitated by hydrogen activation and dissociation on Ni metallic sites, followed by hydrogen spillover to the support, which promotes niobia reduction. To verify this assumption, the degree of reduction was calculated.

When considering the total hydrogen consumption over the entire temperature range, or even only the events at 500 and 675 °C, values well above 100% were obtained. In contrast, a degree of reduction close to 100% was achieved when only the consumption at 500 °C was taken into account. This confirms the attribution of the 500 °C peak to the reduction of NiO to metallic Ni, while the higher-temperature events are likely associated with the partial reduction of Nb_2O_5. These reduction phenomena have been previously reported for a NiO/Nb_2O_5 catalyst, where the TPR profile exhibited a peak associated to NiO reduction between 230 a 430 °C, and two hydrogen consumption peaks above 700°C and 800 °C related to the reduction of Nb_2O_5 [30].

The dispersion of Ni particles on the catalysts was estimated by CO chemisorption (Table 1). Both samples presented same value of CO uptake (0.04 mol_{CO} mol_{Ni}^{-1}), which correspond to a dispersion of around 4% and thus, suggesting the presence of large Ni particles. However, these values do not correspond to the metal particles size derived from XRD analysis. One could speculate that for 5Ni/SBA sample, CO molecules may not assess Ni particles chained in a same pore, while for $5Ni/Nb_2O_5$ sample, Ni particles may be partially covered by NbO_x species which migrates to the surface of nickel during catalyst reduction, due to the strong metal-support interaction (SMSI) effect [31].

Table 1. Physical-chemical properties of Ni-based catalysts.

	Ni wt[a].%	**D[b] Ni (nm)**	**S_{BET}[c] (m^2 g^{-1})**	**Degree of red.[d] (%)**	**CO uptake[e] (mol_{CO} mol_{Ni}^{-1})**
SBA-15	-	-	754	-	-
5Ni/SBA	5.0	8 (7*)	650	98	0.04
Nb_2O_5	-	-	60	-	-
$5Ni/Nb_2O_5$	2.9	8	41	100	0.04

[a] Ni loading (wt.%) measured from ICP-EOS analysis;

[b] Ni metal particle size calculated from XRD of reduced samples; *metal particle size calculated from TEM images;

[c] BET surface area measured by N_2 physisorption analysis;

[d] Degree of reduction for NiO species calculated from the TPR results (considering the peaks at the temperature below 600 °C) and considering the metal content from the ICP-OES analysis;

[e] Content of CO uptake estimated by CO chemisorption analysis.

3.1.2 Catalytic properties for m-cresol transformation

The products distribution and the constant reaction rates for HDO of m-cresol measured at low conversion (around 10%) are listed in Tables 2 and 3, respectively. The bare supports were found to be inactive under the reaction conditions used (300 °C, atmospheric pressure). In contrast, Ni-supported catalysts exhibited notable differences in both activity and selectivity. For the 5Ni/SBA catalyst, the main product formed was 3-methylcyclohexanone (51%), as shown in Table 2. In the case of $5Ni/Nb_2O_5$, toluene was the only product observed. However, this catalyst exhibited a very poor activity since its total reaction rate constant being about eight times lower than that of the silica-based catalyst, with a DDO rate 1.7 times lower (Table 3).

Table 2. Product distribution obtained in the HDO of m-cresol at low conversion ($T_{reaction}$ = 300 °C, 1 atm, 0.5 h on stream).

Catalyst	**W/F (g h mol^{-1})**	**Conversion (%)**	**Selectivity (mol %)**				
			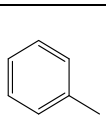	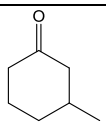	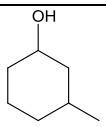	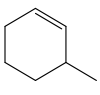	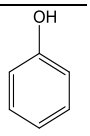
5Ni/SBA	21	9	21	51	18	2	7
$5Ni/Nb_2O_5$	214	11	100	-	-	-	-

Table 3. Reaction rate constant (in mmol g_{Ni}^{-1} h^{-1}) calculated for the global transformation of m-cresol and for each reaction pathway over the Ni-based catalysts ($T_{reaction}$ = 300 °C, 1 atm, 0.5 h on stream).

Catalyst	r_{TOT}	r_{DDO}	r_{HYD}	r_{HYG}
5Ni/SBA	82	17	58	7
5Ni/Nb_2O_5	10	10	-	-

Barrios et al. investigated Pd supported on commercial SiO_2 and Nb_2O_5 for the HDO of phenol under experimental reaction conditions similar to those used in this study (300°C, atmospheric pressure). Reduction steps were between 300 and 500 °C [5]. After the reduction step carried out at 300 °C, the deoxygenated product (benzene) obtained from the DDO route of phenol was mainly produced over Pd supported on niobia (80%) while cyclohexanone (the main product obtained from the HYD route of phenol) was preferentially formed over Pd supported on silica (92%). Trends are then consistent with those reported here with Ni-catalysts (Table 2). Interestingly, the DDO reaction rate was approximately 90 times higher for Pd/Nb_2O_5 compared to Pd/SiO_2 [5]. When the Pd based catalysts were reduced at higher temperatures (until 500 °C), the selectivity into benzene (DDO route) was maintained, however, the DDO rate significantly decreased (by up to 19-fold). The authors attributed the decrease in activity not only to the growth of Pd particles but also to the partial coverage by NbO_x species formed during reduction (an effect similar to the one observed with titania, through the SMSI phenomena). Similar result was reported by Resend et al. with Rh and Ni supported on niobia where authors varied the reduction temperature of the catalysts [20]. In the present study, the constant reaction rate of the 5Ni/Nb_2O_5 catalyst was significantly lower than that of the 5Ni/SBA catalyst, despite both having similar Ni particle sizes and the 5Ni/Nb_2O_5 catalyst exhibiting higher selectivity toward toluene. This suggests that the markedly reduced activity of the 5Ni/Nb_2O_5 catalyst may be attributed to the coverage of Ni particles, a hypothesis supported by the low CO uptake measured for this sample (Table 1).

3.2. Ni-NbO_x dispersed on SBA-15 catalysts: Influence of the Ni/Nb ratio

In an attempt to maximize Ni–NbO_x interface sites while minimizing Ni particle coverage, a series of Ni-NbO_x supported on SBA-15 samples was prepared by varying the Ni and Nb contents. The measured amounts of Ni and Nb in the samples (Table 4) closely matched the expected values, ranging from 2.9 to 5.0 wt% for Ni and from 2.8 to 9.0 wt% for Nb.

The textural properties of the samples are displayed in Fig.2, Fig. S3 and Table 4. All of NiNb/SBA samples presented isotherm type similar to that of the bare SBA-15 support, i.e., type IVa with H1-type hysteresis. This indicates that the mesoporous structure of the support was maintained after infiltration of nickel and niobium precursors followed by thermal treatment. However, discrete differences can be noticed. For the supported materials, the desorption branch is not congruent with the adsorption one, with a latency in its cloture, being more evident for the 2.5Ni5Nb/SBA sample. This is likely due to the filling of NiO and Nb_2O_5 species inside the tubular pores, leading to the partial porosity blockage and decreases in the surface area and pore volume, as evidenced in Table 4. The mesopore and micropore surface areas decreased after metal oxide infiltration, by approximately 25% and up to 65%, respectively. Assuming that NiO and Nb_2O_5 crystallites are confined within the tubular pores of SBA-15, their size should not exceed the pore diameter (~7 nm), which do not agree with the very large crystallites detected in the XRD patterns. This may indicate a heterogeneity in the particles size, with a fraction of particles likely both located within the pores and at the external surface of the silica grains.

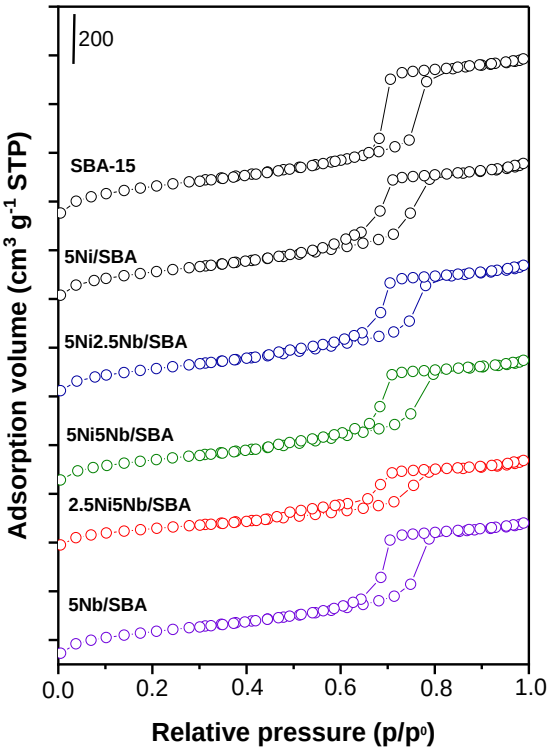

Figure 2. N_2 adsorption-desorption for the NiNb-supported on SBA calcined catalysts

Table 4. Metal loading, textural and physical-chemical properties of the NiNb-based catalysts.

Catalyst	wt[a].%		d[b] (nm)		S_{BET}[c] ($m^2\ g^{-1}$)	S_{micro}[d] ($m^2\ g^{-1}$)	V_p[e] ($m^3\ g^{-1}$)	V_{micro}[f] ($m^3\ g^{-1}$)	D_p[g] (nm)	Degree of red.[h] (%)	CO uptake[i] ($mol_{CO}\ mol_{Ni}^{-1}$)	Total acidity[j] ($\mu mol\ g^{-1}$)
	Ni	Nb	Ni	Nb_2O_5								
5Ni2.5Nb/SBA	4.8	2.8	34	30	608	87	0.87	0.036	6.4	100	0.20	-
5Ni5Nb/SBA	5.0	8.5	38 (3.3*)	30	572	72	0.84	0.028	6.5	102	0.31	20
2.5Ni5Nb/SBA	2.9	4.6	31	27	511	157	0.59	0.069	6.0	99	0.18	14
5Nb/SBA	-	9.0	-	24	625	148	0.91	0.065	6.7	-	-	30

[a] Metal loading (wt.%) measured by ICP-EOS analysis;

[b] Ni(0) and Nb(V) crystallite particle sizes calculated from XRD of reduced samples; *Ni(0) average particle sizes measured by TEM images from reduced samples;

[c] BET surface area; [d] Micropore surface area; [e] Total pore volume; [f] Micropore volume; [g] BJH pore diameter calculated from the desorption branch.

[h] Degree of reduction for the NiO species calculated from the TPR results (considering the peaks at the temperature range from 300 to 700 °C) and considering the metal content from the ICP-OES analysis;

[i] Content of CO uptake estimated by CO chemisorption analysis;

[j] Total acidity obtained from the pyridine adsorption-desorption DRIFTS experiments.

Wide-angle XRD patterns of the catalysts reduced at 500 °C are presented in Fig. 3. In this series of Ni–Nb catalysts supported on SBA-15, narrow diffraction peaks are observed, indicating the presence of large Ni(0) and Nb(V) particles.

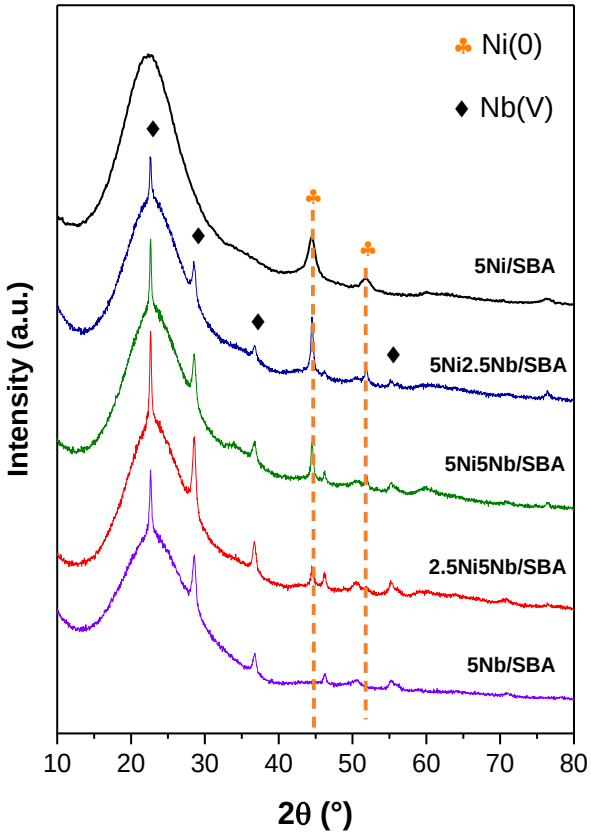

Figure 3. XRD of the reduced NiNb-supported on SBA reduced catalysts.

To obtain precise information on the location and dispersion of NiO and Nb_2O_5 species on the support, HRTEM images of the reduced 5Ni/SBA (Fig. S4) and 5Ni5Nb/SBA (Fig. 4) catalysts were acquired. For the 5Ni/SBA catalyst, it is clearly observed Ni nanoparticles of around of 7 nm confined in the mesopores of the SBA-15, consistent with Ni(0) particle size calculated from XRD of the reduced sample. In the case of 5Ni5Nb/SBA, it is clearly observed the formation of small particles, appearing as agglomerates. Some of these particles may be confined within the mesopores, while others are agglomerated on the external surface of SBA-15. As a result, certain regions of the pore structure remain unfilled. However, from

Figs. 4(a,b), is also noticed in some regions, the formation of few larger particles (varying from 10 to 30 nm) located at the external surface of the SBA-15 grains, which can explain the sharp diffraction peaks of low intensity observed in the XRD pattern of the sample, as well as of those of all the NiNb-supported catalysts. From the histogram of 5Ni5NB/SBA sample (Fig. 4h), particles of size varying mainly from 2 to 4 nm, with an average of 3.3 nm are measured. Besides larger particles being present (> 10 nm), they are not representative in content. EDX elemental mapping of 5Ni5NB/SBA sample (Fig. 5) reveals that Nb element is uniformly dispersed onto the support, with a visible enrichment at the interface with Ni(0) particles confined in the mesopores. In other words, Nb_2O_5 particles appear at the periphery of Ni particles, indicating close spatial contact between the two species.

Metallic sites accessibility was estimated by CO chemisorption analysis, Table 4. The CO uptake varied significantly with catalyst composition. As previously discussed, very low values of CO uptake (0.04 mol_{CO} mol_{Ni}^{-1}) were obtained for 5Ni/SBA and 5Ni/Nb_2O_5 samples, reflecting the hard access of confined Ni particles or partial coverage by the NbO_x species. For the NiNb/SBA samples, values of CO uptake were considerably higher (varying between 0.18 to 0.31 mol_{CO} mol_{Ni}^{-1}), but without any tendency respect to catalyst composition. Indeed, 5Ni5Nb/SBA exhibited a better Ni dispersion (around 30 %) which perfectly agree with the average particle size measured in the TEM images, thus showing that in this case, there is not partial coverage of Ni surface by NbO_x species.

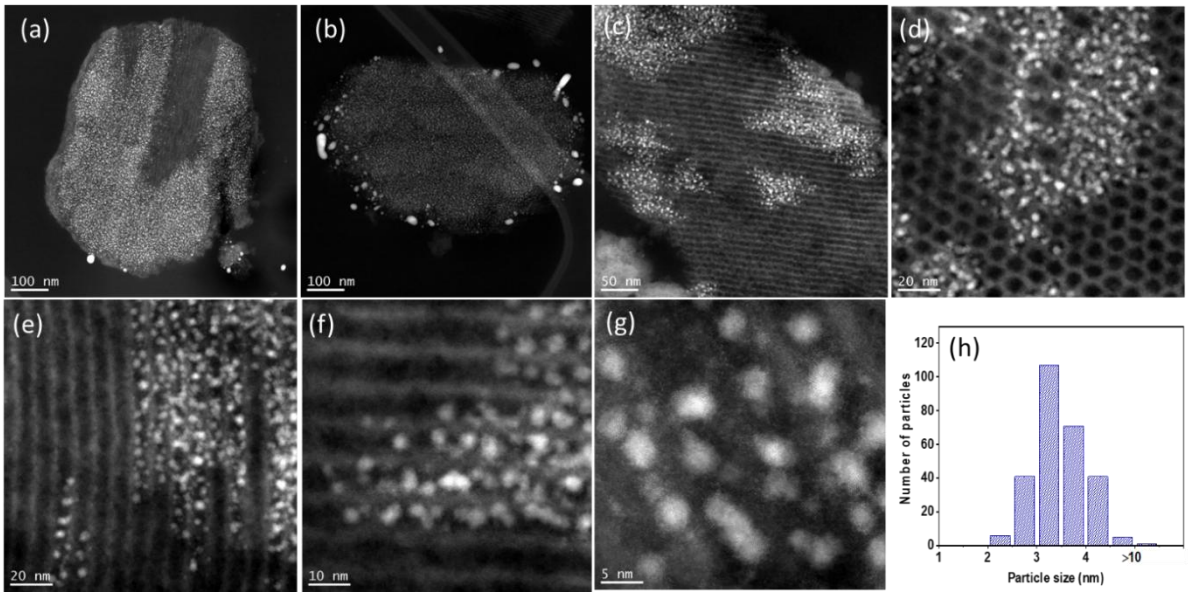

Figure 4. Representative HAADF images of the 5Ni5Nb/SBA reduced catalyst (500 °C, pure H_2, 1h) and the respective particle size distribution.

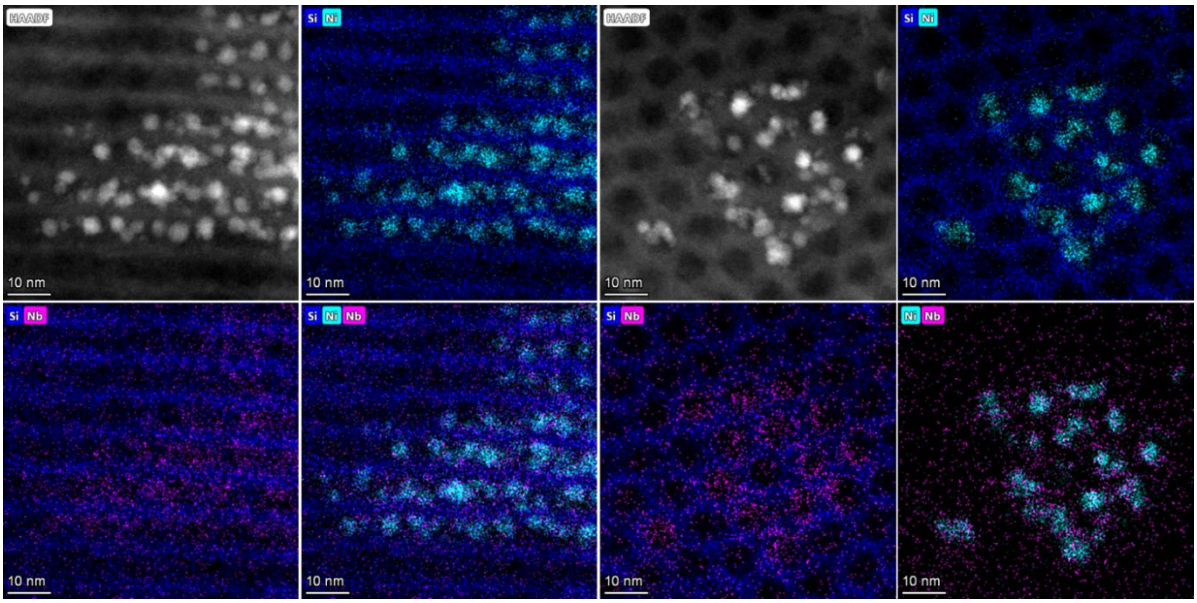

Figure 5. EDXS elemental maps for the 5Ni5Nb/SBA reduced catalyst (500 °C, pure H_2, 1h).

The H_2-TPR profiles of the NiNb/SBA samples are presented on Fig. 6. While the 5Nb/SBA sample shows no noticeable reduction, the NiNb/SBA samples exhibit a complex profile with multiple overlapping reduction peaks, complicating the interpretation. The multiple reduction events are likely associated with reduction of NiO particles of varying

sizes, distributed across different regions of the support, and with various interaction with niobium oxide. All of Ni-Nb supported samples presented quite similar profile, with two main reduction events, with maxima varying between 315-340 °C and 565-600 °C. These peaks are related to the reduction of NiO particles located at the external surface and confined inside the mesopores of the SBA-15, respectively, as also observed in the TPR profile of 5Ni/SBA catalyst (Fig. 1b). A shoulder is also present between 415-435 °C, which may indicate the reduction of Nb-containing NiO domains [32]. Smaller reduction event is detected starting from around 800 °C for all of NiNb-containing samples, which is likely due to the partial reduction of niobium oxide [30,32].

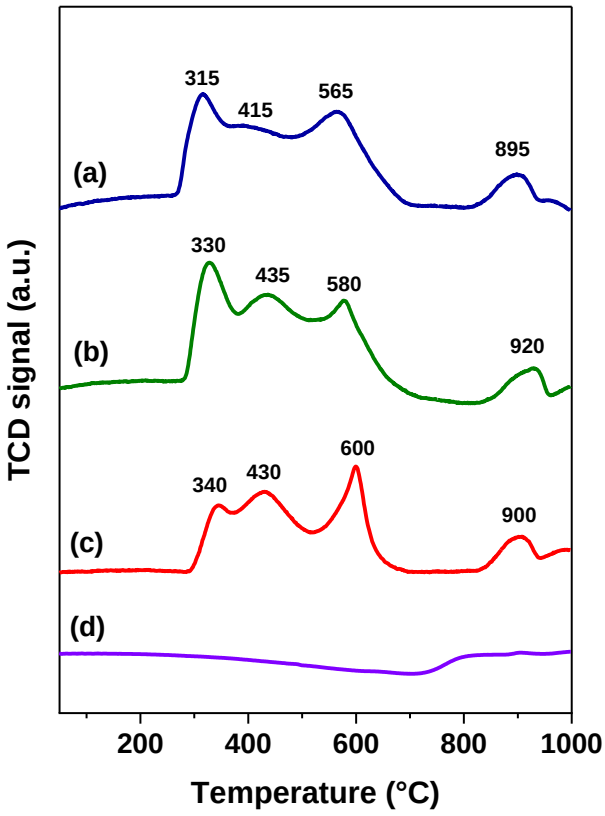

Figure 6. H_2-TPR profiles for the NiNb-supported on SBA-15 samples: (a) 5Ni2.5Nb/SBA, (b) 5Ni5Nb/SBA, (c) 2.5Ni5Nb/SBA and (d) 5Nb/SBA.

The acidic properties of the reduced catalysts were investigated by adsorption-desorption of pyridine analysis (Fig. 7). From the IR spectra after outgassing pyridine at 150

°C (Fig. 7), very low intensity bands are observed for the 5Ni/SBA and 5Ni2.5Nb/SBA samples, indicating the absence or very low acidity for these catalysts. At the opposite, the spectra of the NiNb/SBA samples exhibited:

- well defined bands associated to pyridine adsorbed on Lewis acid sites at around 1450 and 1610 cm^{-1};

- broad and low intensity band at around 1547 cm^{-1} characteristic of Brønsted acid sites;

- band at 1490 cm^{-1} that can be associated with both Lewis and Brønsted acid sites [30].

These results indicate that niobium oxide generates mainly Lewis acid sites, with quantity affected by the Nb_2O_5 content. According to the literature, the type and concentration of acid sites on niobium oxide strongly depends on the temperature of activation, which reflects on its structure and textural properties. Indeed, treating niobia at elevated temperatures (≥ 500 °C) lead to the formation of a crystalline phase of low surface area, thus decreasing the density of exposed acid sites, and dehydroxylating the surface with consequent elimination of Brønsted acid sites [27].

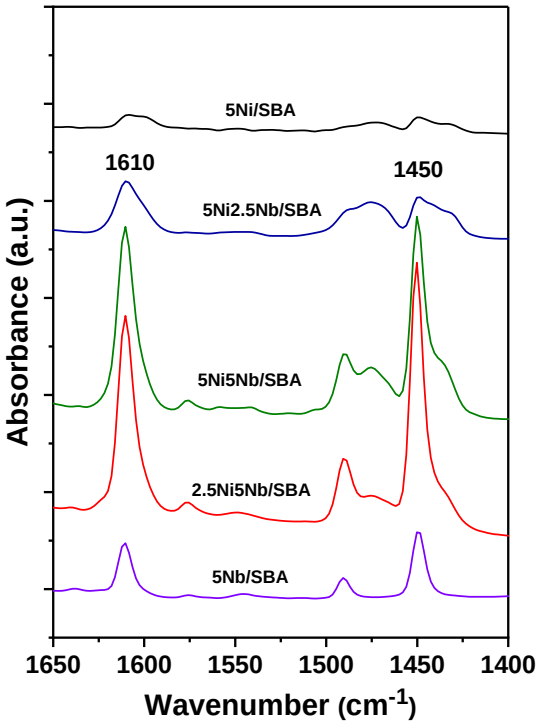

Figure 7. IR spectra of adsorbed pyridine after outgassing at 150 °C.

3.2.2 Catalytic transformation of m-cresol

The transformation of m-cresol over the NiNb/SBA catalysts was evaluated at 300 °C under atmosphere pressure. A comparison on the product distribution obtained at the same level of conversion (~10%) is presented in Table 5. Niobia supported on SBA without Ni (5Nb/SBA) showed no measurable conversion, even at higher W/F values, indicating that metallic sites are essential for activating molecular hydrogen and enabling hydrogenation and hydrogenolysis steps. For Ni-containing catalysts, product selectivity varies significantly with catalyst composition. As previously observed, 3-methylcyclohexanone is the major product obtained (51%) over the 5Ni/SBA catalyst. The introduction of 2.5 wt.% of niobium drastically modified the product selectivity, with toluene becoming the major product (56%). Selectivity toward the ketone and alcohol decreased, while the formation of the respective alkenes and alkane increased. As the niobium content increased further (to 5 wt.%), the selectivity toward the alkenes and alkane remained relatively constant, while toluene formation continued to rise and ketone/alcohol declined. In addition, phenol, produced by hydrogenolysis of m-cresol, was no longer detected at high Nb loading.

Table 5. Product distribution obtained in the HDO of m-cresol (low conversion) over the NiNb-supported on SBA catalysts ($T_{reaction}$ = 300 °C, 1 atm, 0.5 h of time on stream).

Catalyst	**W/F (g h mol^{-1})**	**Conversion (%)**	**Selectivity (mol %)**					
			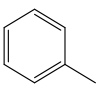	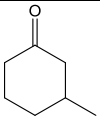	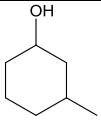	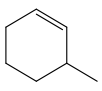	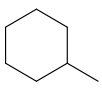	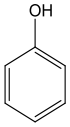
5Ni/SBA	21	9	21	51	18	2	-	7
5Ni2.5Nb/SBA	21	15	56	15	2	14	7	6
5Ni5Nb/SBA	12	15	75	7	-	12	6	-
2.5Ni5Nb/SBA	31	11	67	9	-	13	11	-

From previous investigations on the HDO reaction mechanism of cresol over metals supported on silica and niobia, as well as Ni-based catalysts, different reaction pathways have been proposed, as illustrated in Scheme 1: (i) the direct deoxygenation (DDO) involving the cleavage of the C_{Ar}-O bond to produce toluene; (ii) hydrogenation of the aromatic ring (HYD) to produce methylcyclohexanone and methylcyclohexanol, which may be dehydrated to methylcyclohexene and further hydrogenated to methylcyclohexane; (iii) hydrogenolysis (HYG) of the methyl group of m-cresol to produce phenol and methane. An alternative mechanism with lower energy barrier is the tautomerization of m-cresol, in which a keto-tautomer intermediate can be considered as a common intermediate between the DDO and HYD pathways. Once formed, this instable intermediate may react via two different routes: (i) selective hydrogenation of the C=O bond to produce an unsaturated alcohol which is rapidly dehydrated to toluene or (ii) successive hydrogenation of the C=C bonds followed by same steps previously described for the HYD route. The preference for each reaction pathway is strongly dependent on the nature of the metal and support.

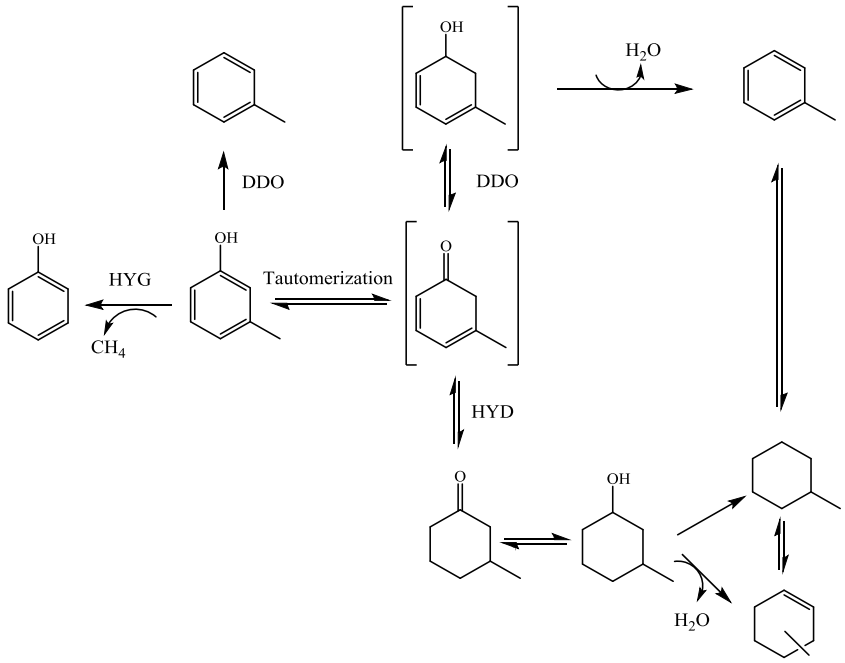

Scheme 1. Reaction pathways proposed for the transformation of m-cresol over the different metal-based catalysts.

For the 5Ni/SBA catalyst, considering the non-acidic or non-oxophilic character of the SiO_2 support and Ni being a hydrogenating metal, the hydrogenation (HYD) pathway is preferred, thus explaining the formation of hydrogenated oxygenated compounds as main products. Besides that, as previously reported, larger Ni particles are also active for hydrogenolysis, a characteristic that can explain the formation of phenol observed in this work for Ni-catalyst [22,31].

Niobia has been identified as an acidic and oxophilic oxide capable of activating the C-O bond in phenolic compounds due to the strong interaction stablished between the Nb^{5+}/Nb^{4+} cations and the oxygen atom [7,36,37]. Incorporating niobium oxide in the perimeter of Ni particles thus facilitates the adsorption and activation of the C-O and/or C=O bond (from the tautomer), thereby lowering the energy barrier for deoxygenation reaction. In order to compare the catalytic performance of monometallic 5Ni/SBA and bifunctional NiNb/SBA catalysts, as well as to evaluate the effect of m-cresol conversion on the product distribution, the W/F values were varied through modification of catalyst weight. Catalysts with lower niobia content, or even reduced Ni content in the presence of niobia, exhibited higher activity than 5Ni/SBA (as evidenced in Fig. 8), thus showing the promoting effect of niobia to the activity of Ni.

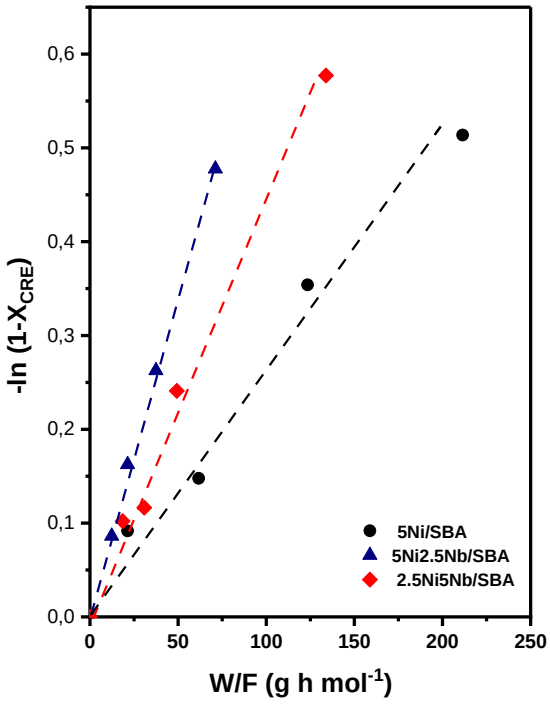

Figure 8. Pseudo-first order plots obtained from the HDO of m-cresol over the Ni-Nb based catalysts at 300 °C, 1 atm, 30 min of TOS.

The product selectivity as a function of m-cresol conversion for 5Ni/SBA, 5Ni2.5Nb/SBA and 2.5Ni5Nb/SBA catalysts are presented in Fig. 9. For the 5Ni/SBA catalyst, as m-cresol conversion increases, selectivity toward 3-methylcyclohexanone and 3-methylcyclohexanol decreases, while selectivity to toluene and phenol rises. This indicates a sequential reaction pathway: the ketone is hydrogenated to the alcohol, which is further converted into methylcyclohexane, and subsequently dehydrogenated to produce toluene. Herein, the formation of methylcyclohexane from the alcohol could proceed via either dehydration to methylcyclohexene followed by hydrogenation, or direct C–OH bond cleavage. Given the weak acidity of Ni/SBA, direct hydrogenolysis is the more likely route. The selectivity to phenol, produced by hydrogenolysis of the methyl group, also increases with conversion, suggesting a competition between hydrogenolysis (HYG) and hydrogenation (HYD) pathways.

For the catalysts containing niobium, regardless of its content, toluene consistently remains the main product across the entire range of conversion. In the case of 5Ni2.5Nb/SBA catalyst, notable differences can be noticed for the minor products with increasing conversion: the selectivity to 3-methylcyclohexanone and methylcyclohexene decreases, while methylcyclohexane and phenol increase. This suggest that 3-methylcyclohexanol undergoes acid-catalyzed dehydration to methylcylohexene, followed by hydrogenation to the corresponding alkane, driven by the acidic nature of niobium oxide. For the 2.5Ni5Nb/SBA catalyst, phenol is never observed even at higher conversion values.

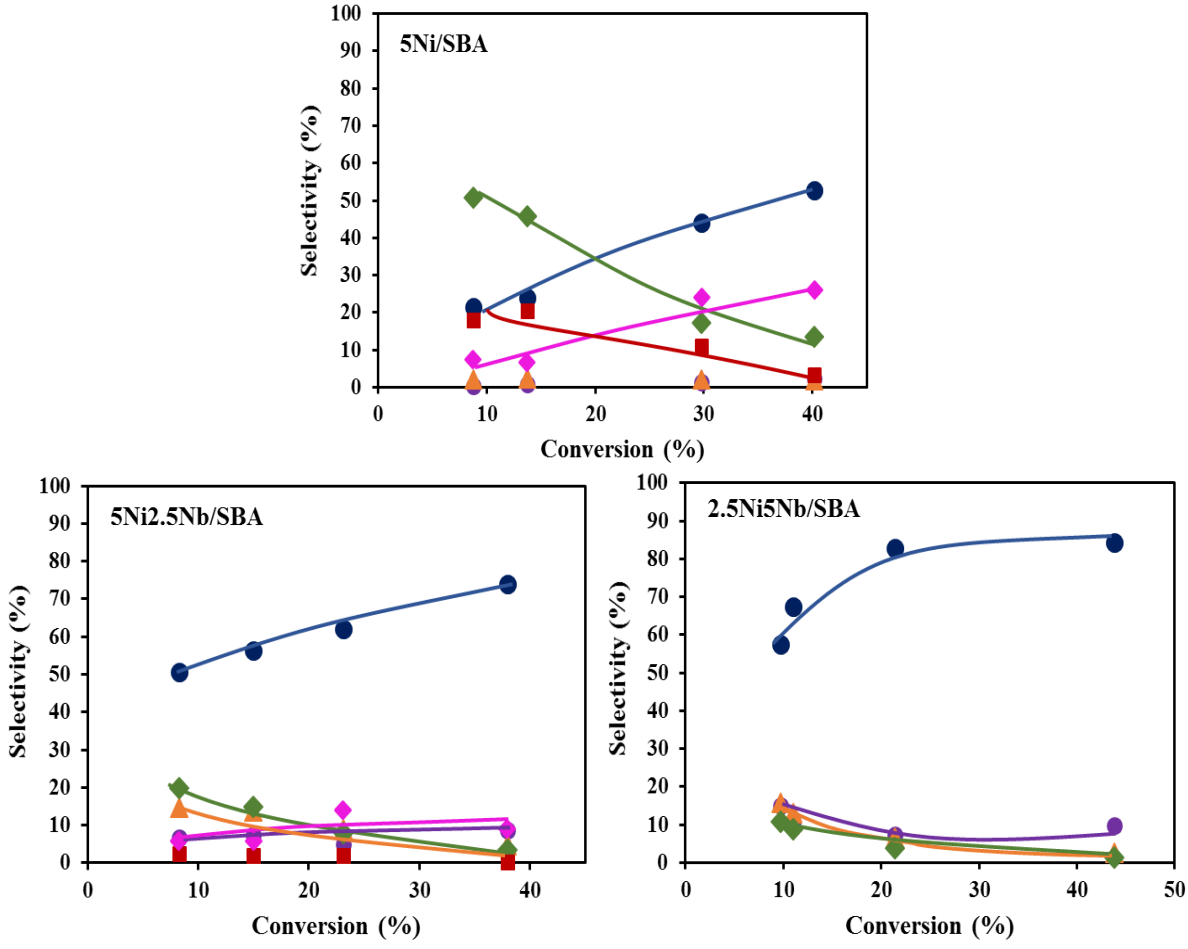

Figure 9. Product selectivity as a function of m-cresol conversion for the Ni-Nb based catalysts. Reaction performed at 300 °C, 1 atm, 30 min of TOS. (●) Toluene, (▲)

methylcyclohexenes, (●) methylcyclohexane, (♦) 3-methylcyclohexanone, (■) 3-methylcyclohexanol, (♦) phenol.

Comparison of the results obtained in this work with those reported in the literature is not straightforward, as reaction conditions (temperature, pressure, and feedstock composition) often differ significantly, strongly influencing the reaction. In addition, variations in catalyst formulation, such as the type of metal and support, also play a crucial role in HDO performance. To address this point, we have selected a number of studies from the literature that, while using different catalysts, were carried out under reaction conditions comparable to those employed in our work. Table 6 summarizes some results selected from the literature on the HDO of m-cresol (at low conversion) performed at temperatures ranging from 250-350 °C and under atmospheric pressure. The product distribution is strongly influenced by the catalyst type. Metals such as Pd, Pt and Ni supported on inert materials such as silica, exhibit higher selectivity toward the hydrogenated product (3-methylcyclohexanone). In contrast, more oxophilic metals such as Ru and Fe or the use of oxophilic supports such as ZrO_2, TiO_2 and Nb_2O_5, favor the deoxygenation, leading to toluene. For Ni-based catalysts, the selectivity toward toluene can be significantly improved by controlling the Ni particle size (smaller particles are more oxophilic and thus promote the DDO pathway), and by combining Ni with oxophilic metals such as Fe and Mo. This observation is consistent with the results obtained in this work, where combining Ni with niobium notably improved deoxygenation. Our 5Ni5Nb/SBA catalyst, which showed the best performance, achieved higher toluene selectivity compared to Ni/SiO_2 catalysts reported in the literature, and exhibited performance comparable to Pd or Pt supported on oxophilic supports. However, it represents a more attractive option, since it relies on non-noble metals.

Table 6. Conversion and product distribution obtained for the HDO of m-cresol at gas phase over different supported metal catalysts reported in the literature.

Catalyst	T (°C)	P (atm)	H_2/m-cresol molar ratio	Conversion (%)	Selectivity (%)				Ref.
					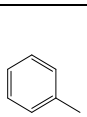	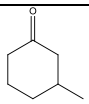	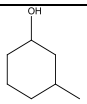		
5Ni5Nb/SBA	300	1	80	15	75	7	-	6	This work
Pd/SiO_2	300	1	60	8.2	3.8	90.3	5.9	-	
Pd/ZrO_2	300	1	60	14.7	80.0	18.4	1.2	0.4	[13]
Pd/TiO_2	300	1	60	7.3	87.9	12.6	-	-	
Pd/Nb_2O_5	300	1	60	13.1	95.6	3.8	-	0.6	
Pd/SBA-15	300	1	60	7.0	38.0	62.0	-	-	[38]
Pd/CeO_2	300	1	60	10.3	19.1	70.5	10.4	-	
$Pd/10SiCeO_2$	300	1	60	15.9	46.8	44.2	9.0	-	[39]
Pd/Fe_2O_3	300	1	-	10.0	~ 87	< 1		-	[40]
Pt/TiO_2	350	1	60	~ 20	~ 100	-		-	[41]
Pt-Nb/C	350	1	-	~ 35	95	-		5	[22]
Pt/SiO_2	300	1	-	7.2	33.3	60.2	6.5	-	[16]
Ru/SiO_2				4.5	38.5	7.4	-	-	
Ni/SiO_2	300	1	60	9.3	46.2	15.1	3.2	-	[42]
Ni/SiO_2	250	1	60	2.3	6.1	52.2	33.0	-	[43]
Fe/SiO_2	300	1	60	8.8	60.2	-	-	-	[10]
$NiFe/SiO_2$				13.7	52.6	-	-	-	
Ni/SiO_2	300	1	90	17.5	46.0	16.5	1.9	2.7	[25]
Ni(1nm)/SBA				22.3	85.7	5.5	0.8	0.6	
$1Ni1Mo/SiO_2$	250	1	60	10.8	83.3	0.0	0.0	5.9	[44]
$Ni0.5Cu/SiO_2$	250	1	50	17.8	20.3	43.5	34.3	0.7	[45]
NiCu(2nm)/SBA	300	1	90	17	85	11	2	-	[46]

*Others products to complete 100 % selectivity includes compounds such as CH_4, C_2-C_5 hydrocarbons, transalkylation products, phenol, depending on the catalyst type.

To further examine the promotional effect of niobium oxide over a Ni-based catalyst, the kinetic rate constants (normalized to Ni content) were calculated for each reaction pathway (Table 6). As can be seen, the DDO rate constant significantly increases with introduction of niobium reaching a maximum with the 5Ni5Nb/SBA catalyst (a 11-fold increase compared to 5Ni/SBA). In contrast, the HYD rate constant remains relatively constant, while the HYG pathway becomes less active and is completely suppressed when Ni and Nb are present in equal proportions. Note that for the HYD rate constant, all of products from the hydrogenation pathway were considered, including methylcyclohexenes and methylcyclohexane. Thus, despite being constant, the HYD rate constant also reflect the formation of deoxygenated aliphatic hydrocarbons. To enable a more meaningful comparison, a DDO factor, defined as the ratio kDDO/(kHYD+kHYG), was calculated in order to represent the relative preference for the DDO pathway over HYD and HYG during the transformation of m-cresol. This factor increased followed the order: Ni/SBA (0.3) < 5Ni2.5Nb/SBA (1.3) < 2.5Ni5Nb/SBA (2.1) < 5Ni5Nb/SBA (3.1). This trend highlights that combining Ni with niobium significantly enhances the deoxygenation activity compared to Ni/SBA, and suggests the existence of an optimum niobium content and/or Ni/Nb ratio to maximize the direct deoxygenation of m-cresol into toluene.

Table 6. Reaction rate constant (in mmol g_{Ni}^{-1} h^{-1}) calculated for the transformation of m-cresol and for each reaction pathway over the Ni-Nb supported on SBA catalysts ($T_{reaction}$ = 300 °C, 1 atm, 0.5 h of time on stream).

Catalyst	r_{TOT}	r_{DDO}	r_{HYD}	r_{HYG}	DDO factor[a]
5Ni/SBA	82	17	58	7	0.3
5Ni2.5Nb/SBA	146	82	55	9	1.3
5Ni5Nb/SBA	249	188	61	0	3.1

2.5Ni5Nb/SBA	123	83	40	0	2.1

[a] The DDO factor was calculated by $k_{DDO}/(k_{HYD}+r_{HYG})$

These results highlight the advantage of combining metallic Ni with niobium oxide species for the deoxygenation of lignin-derived compounds. Nickel, as a transition metal capable of dissociating H_2 , promotes hydrogenation of aromatic rings and/or hydrogenolysis of C–O bonds. However, when used alone, Ni tends to favor ring hydrogenation and C–C hydrogenolysis pathways, yielding mainly alcohols and alkanes rather than achieving direct deoxygenation (DDO) to aromatics. In contrast, niobium in its oxide form (Nb^{5+}/Nb^{4+}), owing to its strong oxophilic character, interacts effectively with oxygen atoms and activates oxygenated functional groups (–OH, $–OCH_3$, C=O). When coupled with metallic sites, these NbO_x species facilitate selective C–O bond cleavage, thereby enhancing the DDO pathway.

Finally, the stability of the catalysts was evaluated during 4 h on stream (TOS) using 5Ni/SBA and 5Ni5Nb/SBA, the last one selected for their superior DDO activity. As shown in Fig. 10, the m-cresol conversion decreased over time for both catalysts, with a higher loss observed for 5Ni5Nb/SBA (31%) compared to 5Ni/SBA (18%), indicating a stronger deactivation of the former, likely linked to the presence of Nb. This trend is consistent with previous reports on Ni-based catalysts for HDO of phenolics under similar conditions (300 °C, 1 atm), where the catalyst deactivation was attributed to the blockage of active sites by coke deposition, intermediates adsorption, and/or Ni particle sintering [25]. To probe these effects, TGA and XRD analyses were performed on both spent catalysts. The TGA profiles (Fig. S5) showed two main losses: the first one below 150°C, attributed to water desorption, and the second between 300 and 600 °C, attributed to the oxidation of strongly adsorbed reaction intermediates (~ 290 °C) and combustion of condensed carbon deposits (400–600 °C) [25,47]. The second loss (between 300 and 600 °C) was much more significant in the case of 5Ni5Nb/SBA, in agreement with the stronger deactivation observed for this catalyst compared

to Ni/SBA (Fig. 10). This suggests that the Nb-promoted catalyst, despite maintaining higher toluene selectivity, is more prone to deactivation by oxygenated species strongly bound to its active sites or by coke formation. The diffractograms of the spent catalysts (Fig. S6) showed a profile similar to that of the reduced samples before the reaction, with 5Ni/SBA maintaining a particle size of around 7 nm. This indicates that metal sintering is not occurring and the strong adsorption of intermediates species on catalyst surface would be the main cause of deactivation. In terms of product distribution, distinct behaviors were observed for both catalysts as already discussed above. Over 5Ni/SBA, toluene selectivity gradually declined with a concomitant increase in methylcyclohexanone and phenol, while for 5Ni5Nb/SBA, the selectivity into toluene, the main product, remained relatively stable.

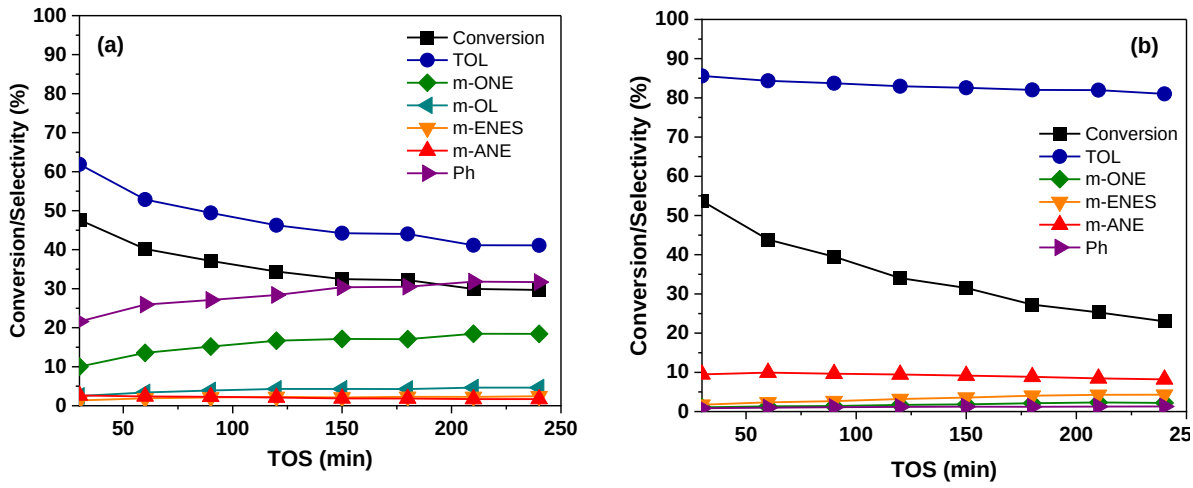

Figure 10. Effect of time on stream on the m-cresol and product distribution over (a) 5Ni/SBA and (b) 5Ni5Nb/SBA catalysts. T: 300°C, P: 1 atm, TOS: 4h.

4. Conclusion

This work evaluated the performance of Ni and Ni-NbO_x interfaces over SBA-15 silica for the gas phase HDO of m-cresol at atmospheric pressure. The results demonstrated that the addition of niobium significantly altered both the activity and product distribution of Ni/SBA

catalyst. While the monometallic Ni catalyst predominantly produced hydrogenated compounds and phenol (via C-C hydrogenolysis), the addition of niobium greatly enhanced toluene formation. In fact, the DDO activity increased by 11-fold with the bifunctional NiNb-supported catalyst, and 18-fold compared to the Ni/Nb_2O_5 catalyst. Although toluene selectivity was lower than that of Ni/Nb_2O_5 catalyst (which achieved 100% of selectivity), the co-dispersion of Ni and NbO_x on silica surface promoted a greater gain in activity. These findings highlight the importance of interfacial Ni-NbO_x sites in promoting the direct deoxygenation pathway. Further optimization of catalysts synthesis procedure to ensure uniform distribution of metal particles size and maximize Ni-NbO_x interfacial sites would lead to highly efficient and cheap catalysts for bio-oil upgrading.

Acknowledgements

This work was performed in the frame of the PYRODEOX project granted by the ANR (ANR-21-CE43-0006). Camila A. Teles and Frederic Richard acknowledge financial support from the European Union (ERDF), "Region Nouvelle Aquitaine". The authors also thank the University of Antioquia, projects Minciencias, ECOSNORD Colombia-Francia, and CODI University of Antioquia 80740-031-2023, 2023-60336. The authors thank Maya Marinova for TEM images. This work likewise pertains to the French government program "Investissements d'Avenir" (EUR INTREE, reference ANR-18-EURE-0010). The Chevreul Institute is thanked for its help in the development of this work through the ARCHI-CM project supported by the "Ministère de l'Enseignement Supérieur de la Recherche et de l'Innovation", the region "Hauts-de-France", and the "Métropole Européenne de Lille.

REFERENCES

[1] D.E. Resasco, S.P. Crossley, Implementation of concepts derived from model compound studies in the separation and conversion of bio-oil to fuel, Catalysis Today 257 (2015) 185–199. https://doi.org/10.1016/j.cattod.2014.06.037.

[2] Y. Luo, V.K. Guda, E.B. Hassan, P.H. Steele, B. Mitchell, F. Yu, Hydrodeoxygenation of oxidized distilled bio-oil for the production of gasoline fuel type, Energy Conversion and Management 112 (2016) 319–327. https://doi.org/10.1016/j.enconman.2015.12.047.
[3] E. Furimsky, Catalytic hydrodeoxygenation, Applied Catalysis A: General 199 (2000) 147–190. https://doi.org/10.1016/S0926-860X(99)00555-4.
[4] Y. Romero, F. Richard, S. Brunet, Hydrodeoxygenation of 2-ethylphenol as a model compound of bio-crude over sulfided Mo-based catalysts: Promoting effect and reaction mechanism, Applied Catalysis B: Environmental 98 (2010) 213–223. https://doi.org/10.1016/j.apcatb.2010.05.031.
[5] A.M. Barrios, C.A. Teles, P.M. de Souza, R.C. Rabelo-Neto, G. Jacobs, B.H. Davis, L.E.P. Borges, F.B. Noronha, Hydrodeoxygenation of phenol over niobia supported Pd catalyst, Catalysis Today 302 (2018) 115–124. https://doi.org/10.1016/j.cattod.2017.03.034.
[6] P.M. de Souza, R.C. Rabelo-Neto, L.E.P. Borges, G. Jacobs, B.H. Davis, T. Sooknoi, D.E. Resasco, F.B. Noronha, Role of Keto Intermediates in the Hydrodeoxygenation of Phenol over Pd on Oxophilic Supports, ACS Catal. 5 (2015) 1318–1329. https://doi.org/10.1021/cs501853t.
[7] C.A. Teles, P.M. de Souza, R.C. Rabelo-Neto, M.B. Griffin, C. Mukarakate, K.A. Orton, D.E. Resasco, F.B. Noronha, Catalytic upgrading of biomass pyrolysis vapors and model compounds using niobia supported Pd catalyst, Applied Catalysis B: Environmental 238 (2018) 38–50. https://doi.org/10.1016/j.apcatb.2018.06.073.
[8] C.A. Teles, R.C. Rabelo-Neto, N. Duong, J. Quiroz, P.H.C. Camargo, G. Jacobs, D.E. Resasco, F.B. Noronha, Role of the metal-support interface in the hydrodeoxygenation reaction of phenol, Applied Catalysis B: Environmental 277 (2020) 119238. https://doi.org/10.1016/j.apcatb.2020.119238.
[9] M.B. Griffin, G.A. Ferguson, D.A. Ruddy, M.J. Biddy, G.T. Beckham, J.A. Schaidle, Role of the Support and Reaction Conditions on the Vapor-Phase Deoxygenation of *m* -Cresol over Pt/C and Pt/TiO $_2$ Catalysts, ACS Catal. 6 (2016) 2715–2727. https://doi.org/10.1021/acscatal.5b02868.
[10] L. Nie, P.M. de Souza, F.B. Noronha, W. An, T. Sooknoi, D.E. Resasco, Selective conversion of m-cresol to toluene over bimetallic Ni–Fe catalysts, Journal of Molecular Catalysis A: Chemical 388–389 (2014) 47–55. https://doi.org/10.1016/j.molcata.2013.09.029.
[11] I.T. Ghampson, G. Pecchi, J.L.G. Fierro, A. Videla, N. Escalona, Catalytic hydrodeoxygenation of anisole over Re-MoO x /TiO 2 and Re-VO x /TiO 2 catalysts, Applied Catalysis B: Environmental 208 (2017) 60–74. https://doi.org/10.1016/j.apcatb.2017.02.047.
[12] P.M. de Souza, R.C. Rabelo-Neto, L.E.P. Borges, G. Jacobs, B.H. Davis, D.E. Resasco, F.B. Noronha, Hydrodeoxygenation of Phenol over Pd Catalysts. Effect of Support on Reaction Mechanism and Catalyst Deactivation, ACS Catal. 7 (2017) 2058–2073. https://doi.org/10.1021/acscatal.6b02022.
[13] C.A. Teles, P.M. de Souza, R.C. Rabelo-Neto, A. Teran, G. Jacobs, D.E. Resasco, F.B. Noronha, Hydrodeoxygenation of Lignin-Derived Compound Mixtures on Pd-Supported on Various Oxides, ACS Sustainable Chem. Eng. 9 (2021) 12870–12884. https://doi.org/10.1021/acssuschemeng.1c03720.
[14] C.A. Teles, R.C. Rabelo-Neto, J.R. de Lima, L.V. Mattos, D.E. Resasco, F.B. Noronha, The Effect of Metal Type on Hydrodeoxygenation of Phenol Over Silica Supported Catalysts, Catal Lett 146 (2016) 1848–1857. https://doi.org/10.1007/s10562-016-1815-5.
[15] C.A. Teles, P.M. de Souza, A.H. Braga, R.C. Rabelo-Neto, A. Teran, G. Jacobs, D.E. Resasco, F.B. Noronha, The role of defect sites and oxophilicity of the support on the

phenol hydrodeoxygenation reaction, Applied Catalysis B: Environmental 249 (2019) 292–305. https://doi.org/10.1016/j.apcatb.2019.02.077.
[16] Q. Tan, G. Wang, L. Nie, A. Dinse, C. Buda, J. Shabaker, D.E. Resasco, Different Product Distributions and Mechanistic Aspects of the Hydrodeoxygenation of m-Cresol over Platinum and Ruthenium Catalysts, ACS Catal. 5 (2015) 6271–6283. https://doi.org/10.1021/acscatal.5b00765.
[17] C. Newman, X. Zhou, B. Goundie, I.T. Ghampson, R.A. Pollock, Z. Ross, M.C. Wheeler, R.W. Meulenberg, R.N. Austin, B.G. Frederick, Effects of support identity and metal dispersion in supported ruthenium hydrodeoxygenation catalysts, Applied Catalysis A: General 477 (2014) 64–74. https://doi.org/10.1016/j.apcata.2014.02.030.
[18] H. Zhao, X. Hu, J. Hao, N. Li, K. Zhi, R. He, Y. Wang, H. Zhou, Q. Liu, An efficient bifunctional Ru-NbOPO4 catalyst for the hydrodeoxygenation of aromatic ethers, phenols and real bio-oil, Applied Catalysis A: General 591 (2020) 117378. https://doi.org/10.1016/j.apcata.2019.117378.
[19] W. Wang, K. Wu, P. Liu, L. Li, Y. Yang, Y. Wang, Hydrodeoxygenation of *p* -Cresol over Pt/Al $_2$ O $_3$ Catalyst Promoted by ZrO $_2$, CeO $_2$, and CeO $_2$ –ZrO $_2$, Ind. Eng. Chem. Res. 55 (2016) 7598–7603. https://doi.org/10.1021/acs.iecr.6b00515.
[20] K.A. Resende, F.B. Noronha, C.E. Hori, Hydrodeoxygenation of phenol over metal supported niobia catalysts, Renewable Energy 149 (2020) 198–207. https://doi.org/10.1016/j.renene.2019.12.061.
[21] R. Huang, O. Kwon, C. Lin, R.J. Gorte, The effects of SMSI on m-Cresol hydrodeoxygenation over Pt/Nb_2O_5 and Pt/TiO_2, Journal of Catalysis 398 (2021) 102-108. https://doi.org/10.1016/j.jcat.2021.04.012.
[22] T. Chen, J.M. Vohs, Direct hydrodeoxygenation of m-cresol to toluene over bifunctional NbO_x-Pt, The Journal of Physical Chemistry C 124, 26 (2020) 14253-14261. https://doi.org/10.1021/acs.jpcc.0c03988.
[23] C. Wang, A.V. Mironenko, A. Raizada, T. Chen, X. Mao, A. Padmanabhan, D.G. Vlachos, R.J. Gorte, J.M. Vohs, Mechanistic Study of the Direct Hydrodeoxygenation of m- Cresol over WO_x- Decorated Pt/C Catalysts, ACS Catalysis 8 (2018) 7749-7759. https://doi.org/10.1021/acscatal.8b01746.
[24] C-Y. Wang, J. Ra, K. Shen, J.M. Vohs, R.J. Gorte, Hydrodeoxygenation of m- Cresol over WO_x- Pt-SBA-15 Using alkanes as hydrogen carriers, ACS Catalysis 13, 16 (2023) 10908-10915. https://doi.org/10.1021/acscatal.3c01636.
[25] C. Abreu Teles, C. Ciotonea, A. Le Valant, C. Canaff, J. Dhainaut, J.-M. Clacens, F. Bellot Noronha, F. Richard, S. Royer, Optimization of catalyst activity and stability in the m-cresol hydrodeoxygenation through Ni particle size control, Applied Catalysis B: Environmental 338 (2023) 123030. https://doi.org/10.1016/j.apcatb.2023.123030.
[26] A. Berenguer, T.M. Sankaranarayanan, G. Gómez, I. Moreno, J.M. Coronado, P. Pizarro, D.P. Serrano, Evaluation of transition metal phosphides supported on ordered mesoporous materials as catalysts for phenol hydrodeoxygenation, Green Chem. 18 (2016) 1938–1951. https://doi.org/10.1039/C5GC02188J.
[27] F. Wang, H-Z. Wu, C-L. Liu, R-Z. Yang, W-S. Dong, Catalytic dehydration of fructose to 5-hydroxymethylfurfural over Nb_2O_5 catalyst in organic solvent, Carbohydrate Research 368 (2013) 78-83. https://doi.org/10.1016/j.carres.2012.12.021.
[28] C. García-Sancho, J.M. Rubio-Caballero, J.M. Mérida-Robles, R. Moreno-Tost, J. Santamaría-González, P. Maireles-Torres, Mesoporous Nb_2O_5 as solid acid catalyst for dehydration of d-xylose into furfural, Catalysis Today 234 (2014) 119-124. https://doi.org/10.1016/j.cattod.2014.02.012.

[29] Z. Zhang, H. Xu, H. Li, Insights into the catalytic performance of Ni-Nb_2O_5 catalysts for vanillin hydrodeoxygenation in aqueous phase: The role of Nb_2O_5 crystal structures, Fuel 324 (2022) 124400. https://doi.org/10.1016/j.fuel.2022.124400.
[30] C. Hernández Mejía, C. Vogt, B.M. Weckhuysen, K.P. de Jong, Stable niobia-supported nickel catalysts for the hydrogenation of carbon monoxide to hydrocarbons, Catalysis Today 343 (2020) 56-62. https://doi.org/10.1016/j.cattod.2018.11.036.
[31] T. Uchijima, SMSI effect in some reducible oxides including niobia, Catalysis Today 28 (1996) 105-117. https://doi.org/10.1016/0920-5861(95)00235-9.
[32] E. Rojas, J.J. Delgado, M.O. Guerrero-Pérez, M.A. Bañares, Performance of NiO and Ni–Nb–O active phases during the ethane ammoxidation into acetonitrile, Catalysis Science & Tecnhology 3 (2013) 3173-3182. https://doi.org/10.1039/C3CY00415E.
[33] C. Hernández Mejía, C. Vogt, B.M. Weckhuysen, K.P. de Jong, Stable niobia-supported nickel catalysts for the hydrogenation of carbon monoxide to hydrocarbons, Catalysis Today 343 (2020) 56-62. https://doi.org/10.1016/j.cattod.2018.11.036.
[34] J. Datka, A.M. Turek, J.M. Jehng, I.E. Wachs, Acidic Properties of Supported Niobium Oxide Catalysts- an infrared spectroscopy investigation, Journal of Catalysis 135 (1992) 186-199. https://doi.org/10.1016/0021-9517(92)90279-Q.
[35] F. Yang, D. Liu, Y. Zhao, H. Wang, J. Han, Q. Ge, X. Zhu, Size Dependence of Vapor Phase Hydrodeoxygenation of *m* -Cresol on Ni/SiO_2 Catalysts, ACS Catal. 8 (2018) 1672–1682. https://doi.org/10.1021/acscatal.7b04097.
[36] S. Kang, R. Miao, J. Guo, J. Fu, Sustainable production of fuels and chemicals from biomass over niobium based catalysts: A review, Catalysis Today 374 (2021) 61–76. https://doi.org/10.1016/j.cattod.2020.10.029.
[37] Q.-N. Xia, Q. Cuan, X.-H. Liu, X.-Q. Gong, G.-Z. Lu, Y.-Q. Wang, Pd/$NbOPO_4$ Multifunctional Catalyst for the Direct Production of Liquid Alkanes from Aldol Adducts of Furans, Angew. Chem. Int. Ed. 53 (2014) 9755–9760. https://doi.org/10.1002/anie.201403440.
[38] C.A. Teles, C. Ciotonea, Nicolas. Gomes, V.O.O. Gonçalves, A. Ungureanu, C. Catrinescu, M. Marinova, J.-M. Clacens, S. Royer, F.B. Noronha, F. Richard, Hydrodeoxygenation of m-cresol over Pd/Al-SBA-15 catalysts: Effect of Al content on the deoxygenation reaction pathways, Applied Catalysis A: General 641 (2022) 118686. https://doi.org/10.1016/j.apcata.2022.118686.
[39] L.R. Francisco, Y. Lyu, C. Sievers, L. Liu, Y. Xing, C.A. Teles, R.C. Rabelo-Neto, L.V. Mattos, F.B. Noronha, The role of oxygen vacancies on the hydrodeoxygenation of lignin-derived compounds over Pd/$SiCeO_2$ catalysts, Applied Catalysis A General 706 (2025) 120497. https://doi.org/10.1016/j.apcata.2025.120497.
[40] Y. Hong, H. Zhang, J. Sun, K.M. Ayman, A.J.R. Hensley, M. Gu, M.H. Engelhard, J.-S. McEwen, Y. Wang, Synergistic Catalysis between Pd and Fe in Gas Phase Hydrodeoxygenation of *m* -Cresol, ACS Catal. 4 (2014) 3335–3345. https://doi.org/10.1021/cs500578g.
[41] X. Zhao, X. Wu, H. Wang, J. Han, Q. Ge, X. Zhu, Effect of Strong Metal-Support Interaction of Pt/TiO_2 on Hydrodeoxygenation of m-Cresol, ChemistrySelect 3, 37 (2018) 10364-10370. https://doi.org/10.1002/slct.201801147.
[42] F. Yang, H. Wang, J. Han, Q. Ge, X. Zhu, Enhanced selective deoxygenation of m-cresol to toluene on Ni/SiO_2 catalysts derived from nickel phyllosilicate, Catalysis Today 330 (2019) 149–156. https://doi.org/10.1016/j.cattod.2018.02.035.
[43] C. Chen, G. Chen, F. Yang, H. Wang, J. Han, Q. Ge, X. Zhu, Vapor phase hydrodeoxygenation and hydrogenation of m -cresol on silica supported Ni, Pd and Pt catalysts, Chemical Engineering Science 135 (2015) 145–154. https://doi.org/10.1016/j.ces.2015.04.054.

[44] F. Yang, N.J. Libretto, M.R. Komarneni, W. Zhou, J.T. Miller, X. Zhu, D.E. Resasco, Enhancement of m- Cresol Hydrodeoxygenation Selectivity on Ni Catalysts by Surface Decoration of MoO_x Species, ACS Catalysis 9 (2019) 7791-7800. https://doi.org/10.1021/acscatal.9b01285.
[45] Y. Wang, H. Wang, J. Han, Q. Ge, X. Zhu, Enhancing direct deoxygenation of m-cresol to toluene through inhibiting C-C hydrogenolysis via alloying Ni with Cu, Chemical Engineering Research and Design, 199 (2023) 49-60. https://doi.org/10.1016/j.cherd.2023.09.023
[46] R. Deplazes, C.A. Teles, C. Ciotonea, P. Simon, E. El Rassi, J. Dhainaut, M. Marinova, N. Canilho, F. Richard, S. Royer, SBA-15 supported Ni-Cu catalysts for hydrodeoxygenation of mcresol to toluene, ChemSusChem 18, 1 (2025) e202400685. https://doi.org/10.1002/cssc.202400685.
[47] C.A. Teles, S. Gueddida, R. Deplazes, C. Ciotonea, N. Canilho, S. Lebègue, J. Dhainaut, M. Badawi, F. Richard, S. Royer, Experimental and Ab initio investigation on the effect of CO and CO_2 during hydrodeoxygenation of m-cresol over Co/SBA-15, ChemCatChem 15, 7 (2023) e202201327. https://doi.org/10.1002/cctc.202201327.